

Accepted Manuscript

Synthesis, structures, spectral properties and DFT quantum chemical calculations of (E)-4-(((4-propylphenyl)imino)methyl)phenol and (E)-4-((2-tolylimino)methyl)phenol; their corrosion inhibition studies of mild steel in aqueous HCl

Elias E. Elemike, Henry U. Nwankwo, Damian C. Onwudiwe, Eric C. Hosten



PII: S0022-2860(17)30360-5

DOI: [10.1016/j.molstruc.2017.03.071](https://doi.org/10.1016/j.molstruc.2017.03.071)

Reference: MOLSTR 23567

To appear in: *Journal of Molecular Structure*

Received Date: 10 January 2017

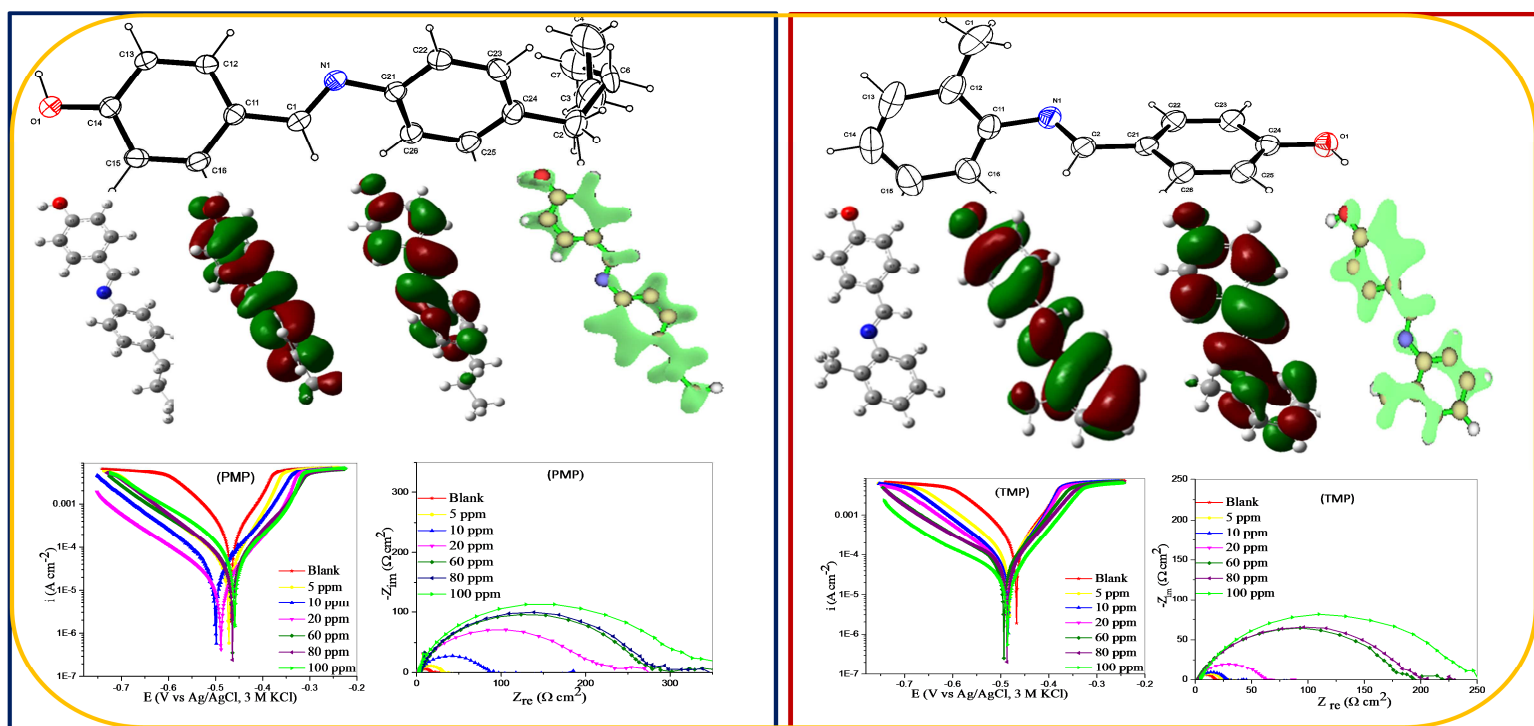
Revised Date: 17 March 2017

Accepted Date: 19 March 2017

Please cite this article as: E.E. Elemike, H.U. Nwankwo, D.C. Onwudiwe, E.C. Hosten, Synthesis, structures, spectral properties and DFT quantum chemical calculations of (E)-4-(((4-propylphenyl)imino)methyl)phenol and (E)-4-((2-tolylimino)methyl)phenol; their corrosion inhibition studies of mild steel in aqueous HCl, *Journal of Molecular Structure* (2017), doi: 10.1016/j.molstruc.2017.03.071.

This is a PDF file of an unedited manuscript that has been accepted for publication. As a service to our customers we are providing this early version of the manuscript. The manuscript will undergo copyediting, typesetting, and review of the resulting proof before it is published in its final form. Please note that during the production process errors may be discovered which could affect the content, and all legal disclaimers that apply to the journal pertain.

GRAPHICAL ABSTRACT



Synthesis, structures, spectral properties and DFT quantum chemical calculations of (E)-4-(((4-propylphenyl)imino)methyl)phenol and (E)-4-((2-tolylimino)methyl)phenol; their corrosion inhibition studies of mild steel in aqueous HCl

Elias E. Elemike^{1,2,3}, Henry U. Nwankwo^{1,2}, Damian C. Onwudiwe^{*1,2}, Eric C. Hosten⁴

1. Material Science Innovation and Modelling (MaSIM) Research Focus Area, Faculty of Agriculture, Science and Technology, North-West University, Mafikeng Campus, Private Bag X2046, Mmabatho 2735, South Africa.
2. Department of Chemistry, School of Mathematics and Physical Sciences, Faculty of Agriculture, Science and Technology, North-West University, Mafikeng Campus, Private Bag X2046, Mmabatho 2735, South Africa.
3. Department of Chemistry, College of Science, Federal University of Petroleum Resources, P.M.B 1221, Effurun, Delta State, Nigeria.
4. Department of Chemistry, Nelson Mandela Metropolitan University, P.O. Box 77000, Port Elizabeth 6031, South Africa

* Corresponding author

Email: Damian.Onwudiwe@nwu.ac.za

Tel: +27 18 - 389 -2545; Fax: +2718 – 389 -2420

Abstract

Two Schiff base compounds with similar backbone, but different positions and lengths of alkyl groups, (E)-4-(((4-propylphenyl)imino)methyl)phenol (PMP) and (E)-4-((2-tolylimino)methyl)phenol (TMP) have been synthesized. Their structures were established by spectroscopic techniques which include FTIR, ¹H and ¹³C-NMR, relative molecular mass (mass spect.), and X-ray crystallography. The spectroscopic methods revealed the characteristic imine functional groups and the exact molecular masses of the compounds. Single crystal analysis revealed an orthorhombic crystal system with Pca21 space group for the two compounds; and the structure of PMP reveal that the propyl group is disordered over two positions in 0.79:0.21 ratio. The corrosion inhibition behaviour of the two Schiff bases were studied by electrochemical measurements. The results suggest that the two derivatives

adsorbed onto the mild steel surface and formed hydrophobic films, which to an appreciable extent, protected the surface of the mild steel. Potentiodynamic polarization results strongly suggested that the investigated Schiff bases behave as mixed-type inhibitors with a more pronounced cathodic nature, and the adsorption isotherm basically obeys the Langmuir isotherm. Quantum chemical computations were also employed to provide further explanations on the adsorption mode, and the theoretical predictions conformed to the experimental results.

Keywords: Crystal structure; schiff base compounds; quantum chemical calculations; corrosion inhibition

1.0 Introduction

The rich chemistry of Schiff bases which centers on the azomethine functional group play critical role in the understanding and fine tuning of their applications [1]. The growing interest in this class of compounds is, to a large extent, due to their structural resemblance with naturally occurring biological molecules, relatively easy synthetic routes and synthetic flexibility that give room for the design of required structural properties. Schiff base compounds are very common intermediates for the preparation of arylacetamide, azetidinone, formazone, thiazolidinone, including metal complexes and other derivatives [2, 3].

Synthesis of this type of carbon-nitrogen double bond requires careful procedure and has involved methods such as solvent based, mechano-chemical or solvent-free and microwave assisted methods but there is low yield and pH specifications associated with solvent based methods. pH scale for such reactions normally span between 5 to 8 depending on the basic nature of the amines [4]. In mechano-chemical synthetic method, Tella *et al* have applied

ball-milling technique in the absence of solvent, for 20 min, to synthesize trimethoprim complexes of Cu(II) and Ni(II) [5]. The microwave assisted synthetic method has proved to be rapid and efficient involving solventless medium with high yield of products [6].

The increasing interest in imine compounds is associated with their presence in many biological systems. They have found applications in organic synthesis, chemical catalysis, medicine, pharmacy, chemical analysis, cation carriers in potentiometric sensors and as corrosion inhibition agents [7-18]. Some of the applications in medicine and pharmacy include use as antitumor, anti-inflammatory, antiviral, antifungal and antibacterial agents, and in the treatment of cancer, HIV and diabetes, and also immobilization of enzymes [8-18]. Investigations focusing on the catalytic properties of Schiff bases have recorded success in the hydrogenation of olefins. Moreover, due to their photo, thermochromic and optical non-linearity properties, they have immense applications in modern technology ranging from optical computers, detection and monitoring of the intensity of radiation, imaging systems, optical sound recording technology, molecular memory storing systems, as organic materials in reversible optical memories and optical detectors in biological systems, photostabilizers, dyes for solar collectors and solar filters [19, 20]. Schiff bases can create the platform for application as efficient molecular conductors using electrical properties to proton transfer [21, 22]. Because of their high catalytic properties, they are employed in photoelectrochemical processes, serving great modification to electrode materials, micro-electronic devices, organic batteries or graphical output devices [23]. Another interesting application of these compounds, especially in this present study, is their use as efficient corrosion inhibitors. The mode of action of an excellent corrosion inhibitor involves the spontaneous formation of impervious system on the surface of interest [24]. The adsorption of Schiff base molecules onto metal components is made possible by the presence of the imine group, the electron

cloud present in the aromatic ring and other electronegative atoms which might be present [25].

Most recently, density functional theory (DFT) has been broadly used in theoretical modelling to provide deep understanding of molecular properties of compounds through the development of exchange–correlation functionals in addition to its great accuracy in replicating the experimental parameters such as in geometry, dipole moment, and vibrational frequency [26-29].

Schiff base ligands derived from the condensation of 4-propylaniline and 2-methylaniline with 4-hydroxybenzaldehyde are presented in this study. Spectral properties of the compound would be investigated using $^1\text{H-NMR}$, $^{13}\text{C-NMR}$, FTIR and mass spectroscopies. Single crystal x-ray analysis of the structures are carried out, and the optimized molecular geometries obtained by using theoretical models. Their electrochemical activity will be investigated using potentiodynamic polarization (PDP) and electrochemical impedance spectroscopy (EIS). The potentials of the compounds as corrosion inhibitors on mild steel are investigated by determining the degree of protection offered by the molecules of the compounds on mild steel in HCl medium. The interest on Schiff base among other corrosion inhibitors is due to their inherent advantages such as green techniques, reduced toxicity, enhanced safe level, ease of adherence onto steel surface, inexpensiveness, simple synthetic route and excellent inhibition efficiency [30]. Furthermore, the effect of the different alkyl groups on the ortho and para positions of the aromatic ring would provide insight into their atomic and molecular behaviour; thereby shed light on their potential inhibition efficacies. The crystal structures of these molecules are reported for the first time in this research and evaluation of their corrosion inhibition properties has not been reported elsewhere.

2.0 Materials and methods

2.1 Materials and physical measurements

The reagents, 4-propylaniline, 4-hydroxybenzaldehyde, o-toluidine and solvents used in this work were of analytical grade and purchased from Sigma–Aldrich and Merck companies. They were used without further purification. FTIR spectra of the synthesized ligands and the adsorbed film of the ligands on mild steel surface, after immersion in acidic solution containing 100 ppm Schiff base for 3 h, were recorded on a Bruker alpha-P FTIR spectrophotometer in the wavenumber range 400 – 4000 cm^{-1} . ^1H and ^{13}C NMR measurements were performed on 600 MHz Bruker Avance III NMR spectrometers at room temperature using DMSO as solvent. The molecular masses of the ligands were determined using micrOTOF-Q 11 10390 Bruker compass Mass spectrometer. All electrochemical measurements were performed using AUTOLAB Potentiostat PGSTAT 302 (Eco Chemie, Utrecht, Netherlands) driven by the NOVA software version 1.10 in an electrochemical workstation which consists of conventional three-electrode cell assembly system with a mild steel as the working electrode, a silver-silver chloride with 3 M KCl as the reference electrode, and a platinum (Pt) rod as the counter electrode.

2.2 Synthesis of (E)-4-(((4-propylphenyl)imino)methyl)phenol (PMP) and (E)-4-((2-tolylimino)methyl)phenol (TMP)

In a general synthesis procedure, to a mixture of 1.20 g (10 mmol) p-hydroxybenzaldehyde in 20 mL ethanol, 1.50 mL (10mmol) 4-propylaniline in 20 mL ethanol was added with drops of glacial acetic acid to give PMP. Similarly, in another reaction for TMP, 1.10 mL (10 mmol) o-toluidine in 20 mL ethanol was mixed with 1.20 g (10 mmol) p-hydroxybenzaldehyde in 20

mL ethanol with added drops of glacial acetic acid. The solutions were separately refluxed with stirring. After 2 h, the resulting clear solutions were filtered and kept at room temperature for slow evaporation. Fine yellow crystals suitable for single crystal X-ray analysis were obtained after 5 days.

PMP: yield 47.5%, M.pt. 148-150 °C. Selected IR (cm⁻¹): 3366(OH stretch), 3024 ν(C-H aromatics), 2954, 2922, 2857 ν(sp³C-H), 2584 ν(HC=N), 1497ν(C=C), 1264, 1205 ν(C-O), 977 σ(O-H), 887, 836, 793 σ(p-OH). ¹H NMR (DMSO, ppm, 600 MHz): δ = 0.84 -0.88 (m, CH₃), 1.49 - 2.05 (m, 6H), 2.31 - 2.54 (m, 3H), 6.45 - 7.78 (m, C₆H₄), 8.46 (s, N=CH), 9.82 (s, OH). ¹³C NMR (DMSO, δ ppm): δ = 11.89(CH₃), 16.54(CH₂), 39.25(CH₂), 114.05, 115.20, 120.65, 129.05, 130.35, 132.30, 140.01, 145.75, 149.67, 159.33, 160.60 (C₆H₄), 161.73 (HC=N), 191.16 (C-OH). MS (ESI) m/z = C₁₆H₁₇NO Calcd. 239.29. Found [M+H]⁺ = 240.14 (100%). Anal. Calc. for C₁₆H₁₇NO: C, 80.30; H, 7.16; N, 5.85; Found: C, 81.09; H, 6.98; N, 6.15%.

TMP: yield 50.3%. M.pt. 172-175°C. Selected IR (cm⁻¹): 3051, 3019 ν(C-H aromatics), 2865, 2822 ν(sp³ C-H), 2722 ν(HC=N), 1485 ν(C=C), 1269, 1215 ν(C-O), 997 σ(OH), 863, 782, 754 σ(p-OH). ¹H NMR (DMSO, ppm, 600 MHz): δ = 2.24 (s, CH₃), 6.44 (s, 1H), 6.65 (s, 1H), 6.81-7.09 (m, C₆H₄), 7.19 (s, 2 H), 7.78 (d, 2H), 8.31 (s, 1H), 9.77 (s, OH); ¹³C NMR (DMSO, ppm, 600 MHz): δ 17.84 (CH₃, C-7), 116.19 (C-6), 117.97 (C-14), 126.59 (C-3), 130.69(C-3, C-11, C-15), 146.64(C-10), 151.22(C-4), 159.55(C-5), 160.63(-C=N), 191.19(C-OH). MS (ESI) m/z = C₁₄H₁₃NO Calcd. 211.26. Found [M+H]⁺ = 212.11 (100%). Anal. Calc. for C₁₄H₁₃NO: C, 79.59; H, 6.20; N, 6.63; Found: C, 80.05; H, 6.44; N, 6.54%.

2.3 X-ray crystallography

X-ray diffraction studies were carried out at 200 K using a Bruker Kappa Apex II diffractometer with graphite monochromated Mo K α radiation ($\lambda = 0.71073 \text{ \AA}$). APEXII and SAINT were used for data collection, cell refinement and data reduction [31]. Structural elucidation were carried out using SHELXT-2014[32], and improved by least-squares methods using SHELXL-2014 with SHELXLE as a graphical interface [32, 33]. Carbon-bound H atoms were placed in calculated positions and were incorporated in the refinement in the riding model approximation, with $U_{\text{iso}}(\text{H})$ set to $1.2U_{\text{eq}}(\text{C})$ while all non-hydrogen atoms were refined anisotropically. There was rotation of the H atoms of the methyl group with a fixed angle around the C—C bond in order to give excellent fit to the experimental electron density (HFIX 137 in the SHELX program suite,³² with $U_{\text{iso}}(\text{H})$ set to $1.5U_{\text{eq}}(\text{C})$. Similar rotation was equally allowed for the hydroxyl H around the C—O bond to best fit the experimental electron density (HFIX 147 in the SHELX program suite [32], with $U_{\text{iso}}(\text{H})$ set to $1.5U_{\text{eq}}(\text{O})$. The propyl group is disordered and necessitates the utilization of various constraints. The data were corrected for absorption effects by the numerical method using SADABS [31].

2.4 Electrochemical techniques

The complete electrochemical setup was allowed to reach the steady state, followed by potential scan conducted for 1800 s in the aggressive solutions which contained various concentrations of inhibitors and also a control (without inhibitor). Subsequently, potentiodynamic polarization (PDP) measurements were carried out after 1800 s of mild steel immersion in the aggressive solutions by sweeping the potential in the range of -0.25 to +0.25 V at the scan rate of 0.5 mVs^{-1} . The corrosion current density (i_{corr}), anodic and cathodic Tafel slopes (β_{a} and β_{c} respectively) were obtained from the polarization curves by

extrapolating the linear Tafel segments to the corrosion potential (E_{corr}). The inhibition efficiency ($\eta\%$) was, thereafter, obtained. Electrochemical impedance spectroscopic (EIS) techniques were carried out at the OCP by analysing the frequency response of the electrochemical system in the range 10 mHz to 100 kHz at 10 mV root-mean-square (rms) amplitude. The impedance spectra were fitted into appropriate equivalent circuit to obtain required electrochemical data such as the charge transfer resistance (R_{ct}).

2.5 Quantum chemical calculations details

Gaussian 09 software was used to calculate the quantum chemical parameters necessary to explain the atomic and molecular interactions involved in the compounds. Density functional theory (DFT) approach, which involves the Becke's three-parameter hybrid functional and Lee-Yang-Paar correlation functional (B3LYP) combined with the 6-31 G+(d) basis function was used to obtain the optimized structures [34]. The DFT, among other functions, has shown excellent promise in revealing the changes in electronic structure responsible for inhibitory action of compounds on metal surfaces. GaussView 5.0 software was further applied in visualizing the electron density graphical isosurfaces and the quantum chemical parameters such as the energy of the highest occupied molecular orbital (E_{HOMO}), the energy of the lowest unoccupied molecular orbital (E_{LUMO}), the energy gap ($\Delta E = E_{\text{HOMO}} - E_{\text{LUMO}}$), chemical potential (μ), absolute hardness (χ), absolute softness, nucleophilicity index (N) and fraction of electron transfer from the inhibitor to the metal surface (ΔN), were quantified using equations 1-7 [35, 36].

$$I_p \text{ (Ionization potential)} = -E_{\text{HOMO}} \text{ and } E_A \text{ (electron affinity)} = -E_{\text{LUMO}} \quad (1)$$

$$\text{Chemical potential, } \mu = -\frac{1}{2}(I_p + E_A) \quad (2)$$

$$\text{Absolute hardness, } \chi = -\frac{1}{2}(E_{\text{HOMO}} - E_{\text{LUMO}}) \quad (3)$$

$$\text{Energy gap } \Delta E = E_{\text{LUMO}} - E_{\text{HOMO}} \quad (4)$$

$$\text{Nucleophilicity index (N)} = \frac{1}{\omega} \quad (5)$$

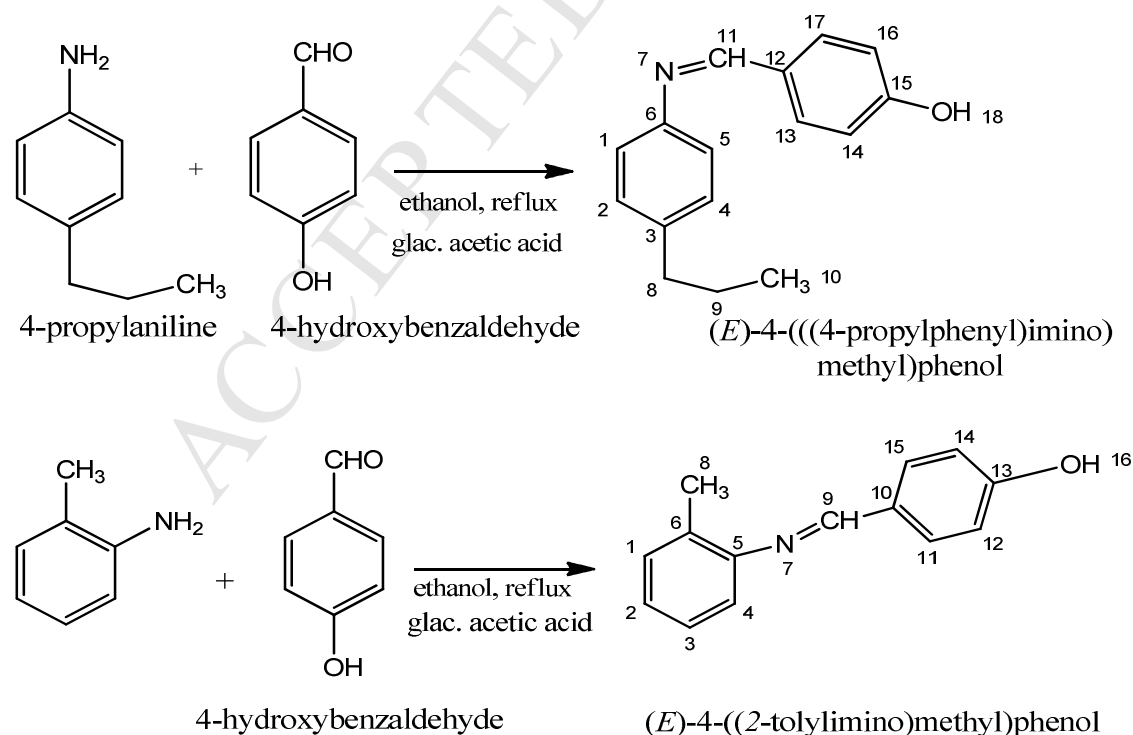
$$\text{Global softness } (\sigma) = \frac{1}{\chi} \quad (6)$$

$$\text{Amount of } e^- \text{ which migrates inhibitor to metal surface } (\Delta N) = \frac{\eta_{Fe} - \eta_{inh}}{2(\chi_{Fe} + \chi_{inh})} \quad (7)$$

3.0 Results and discussion

3.1 Synthesis

A condensation reaction between 4-propylaniline and 4-hydroxybenzaldehyde (1:1 molar ratio) in ethanol afforded (E)-4-(((4-propylphenyl)imino)methyl)phenol (PMP), while similar reaction between o-toluidine and 4-hydroxybenzaldehyde gave (E)-4-((2-tolylimino)methyl)phenol (TMP) as presented in scheme 1. Both compounds were obtained at moderately high yield, are brownish yellow in colour and stable at ambient conditions. The structures were elucidated using spectroscopic techniques and confirmed by X-ray crystallography. The mass spectra results gave molecular ion peaks at 240.14 and 212.11 for PMP and TMP respectively. Experimental and theoretical results were in agreement with each other and confirmed the structures of the compounds.



Scheme 1: Synthesis route for the compounds, PMP and TMP.

3.2 FTIR measurements

The spectra of both compounds, presented in Figures 1a and 1b, showed the absence of bands due to NH_2 and CO groups of the starting materials and the presence of bands due to the azomethine group. The band which appeared around 3366 cm^{-1} could be assigned to the vibrational frequency due to the phenolic OH [37]. The stretching vibrations around 3024 cm^{-1} (for PMP) and 3019 cm^{-1} (for TMP) are due to C-H of the aromatic rings. The three weak bands observed at 2954, 2922, 2857 for PMP are sp^3 CH vibrations attached to the aromatic ring. They were similarly observed in the range 2822 and 2865 cm^{-1} for TMP. Two strong absorption bands which occurred around 1265 and 1205 for PMP; and around 1269 and 1215 for TMP could be attributed to the O-H deformation modes and C-O stretching vibration respectively. Sharp and intense bands characteristic of the vibrations of $\nu(\text{C}=\text{C})$ and $\nu(\text{CH}=\text{N})$ were noticed around 1898 and 1604 cm^{-1} for PMP, while for TMP they occurred around 1681 and 1625 cm^{-1} [38]. The O-H bending vibration in PMP and TMP were observed around 977 and 997 cm^{-1} respectively. The sharp bands around 887, 836, 782, and 754 in the spectra of both compounds are diagnostic peaks attributed to p-substituted OH derivative of aromatic ring [39].

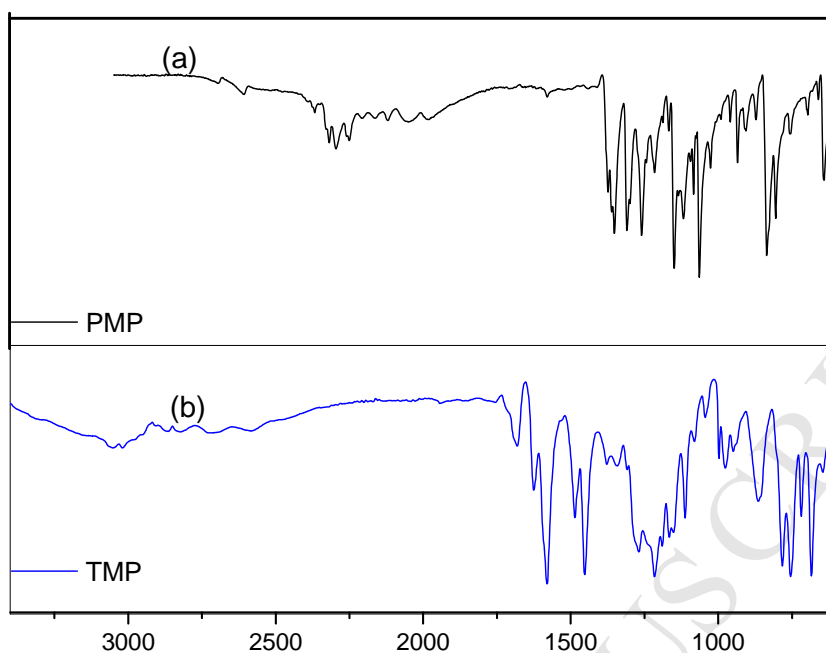


Figure 1: FTIR spectra of the synthesized Schiff base ligands

3.3 NMR spectroscopy

In the ^1H NMR spectra, the chemical shifts due to the aromatic protons, the hydroxyl protons and protons due to alkyl substituents were clearly observed. The proton due to the $\text{HC}=\text{N}$ group appeared as singlet at 8.46 and 8.31 ppm for PMP and TMP, respectively. The hydroxyl group bounded to the aromatic ring showed signals at 9.85 for PMP and 9.77 ppm for TMP. The positions of these peaks reflect the electronegative property of the aromatic ring, and possible presence of hydrogen bonding leading to downfield resonance [39]. PMP showed peaks in the range 0.81 - 0.88, 1.49 - 2.05, and 2.31 - 2.54 ppm, which are due to the terminal CH_3 , CH_2 at position 9, and the protons of the CH_2 at position 8 respectively. In the spectrum of TMP, the signals observed at 2.24 ppm could be due to protons of CH_3 at position 7. The aromatic protons appeared as multiplets and were observed between 6.44-7.78 ppm in both compounds. The protons at positions 13 and 17 for PMP are chemically equivalent and

resonated at 7.78 ppm, and similar situations were observed for the protons at positions 11 and 15 of TMP. Other protons with equivalent environments are found at positions 1 and 5, 2 and 4, 14 and 16 for PMP and 12 and 14 for TMP.

In the ^{13}C -NMR spectra, the compounds showed signals in the region 11.00-191.00 ppm with varied intensities which signify the type of carbon atom. The signals due to the phenyl group were observed in the aromatic region between 110 and 160 ppm, and the position is a function of the proximity of the carbon atoms to different electron donating or withdrawing groups [39]. Signals at 161.73 and 160.63 ppm in the spectra of PMP and TMP respectively are ascribed to the C=N functional group. PMP showed CH_3 signals at 11.89, and the signals due to the CH_2 at position 9 and 8 at 16.54 and 39.25 ppm respectively. In the spectrum of TMP, the signal found at 17.84 ppm could be attributed to the CH_3 attached to the aromatic ring. A low intensity signal observed at 191.19 ppm in the spectra of both compounds is ascribed to the carbon atoms bearing the OH group, and the enhanced downfield shift is due to its para-position. The signals due to carbons at position 6 in PMP and the carbon at position 5 in TMP were observed at 160.60 ppm and 159.55 ppm respectively. The proximity of these carbons to the electronegative nitrogen atom enhances their deshielding effect and caused them to resonate at higher δ -values [39]. Other aromatic carbons appeared in the range 115 to 151.22 ppm. Among the aromatic carbons, C-14, C-16 and C-1, C-5 for PMP showed signals at 114 and 120 ppm respectively, while for TMP the C-6, C-12 and C-14 showed their signals in relatively up-field regions: 116 to 117.97 ppm. This is because in TMP these carbons are in β -positions to the electron withdrawing groups: N and OH, thereby experiencing some deshielding effect. The highest observed peaks for PMP are at 114.05 and 129.05 ppm, and are assigned to C-16 and C-1 respectively.

3.4 X-ray crystallography

An ORTEP structures and the crystal packing of PMP and TMP with the atom-numbering scheme is presented in Figures 2 and 3 respectively. Table 1 presents the crystallographic data of the compounds. Selected bond distances and angles are summarized in Table 2. Both compounds crystallized in an orthorhombic crystal system with space group Pca21. In the asymmetric unit there are four molecules of the compounds. The structure of PMP is non-planar, with the least square plane through the phenol ring making a dihedral angle of $51.61(9)^\circ$ with the least square plane through the propylbenzene ring. The propyl group is disordered over two positions in a 0.79:0.21 ratio. The least square plane through both propyl groups makes a dihedral angle of $84.6(8)^\circ$ with the propylbenzene. There is one intermolecular O1—H1A...N1i (i: -x,1-y,1/2+z) interaction of length 1.88 Å which links adjacent molecules and can be described with a C11(8) graph-set descriptor on the unary level [40, 41]. There is no short $\pi\cdots\pi$ ring interactions, but there are two longish C—H... π ring interactions with hydrogen to centroid length of 2.82 and 2.87 Å with the phenol and propylbenzene rings respectively.

The structure of TMP shows that the N1-C2 bond length (1.2740) conforms to the double bond for the imine group, while the N1-C11 (1.436) bond length agrees with the single bonds for the amine groups [42]. Similar to the PMP, the structure of TMP is non-planar with the least square plane through the phenol ring, making a dihedral angle of $77.44(8)^\circ$ with the least square plane through the toluene ring. There is an intermolecular O1—H1...N1i (i: 1/2+x,1-y,z) interaction of length 1.92 Å which links adjacent molecules and can be described with a C11(8) graph-set descriptor on the unary level [40, 41]. There is also a long C26—H26...O1ii (ii: 2-x,1-y,1/2+z) interaction of length 2.53 Å. There are no short $\pi\cdots\pi$ ring or X—H... π ring interactions.

Table 1: Crystallographic data, data collection and structure refinement for the ligands

compound	(E)-4-(((4-propylphenyl)imino)methyl)phenol	(E)-4-((2-tolylimino)methyl)phenol
CCDC	1527670	1491358
Empirical formula	C ₁₆ H ₁₇ NO	C ₁₄ H ₁₃ NO
Colour/shape	yellow	yellow
Formular weight	239.31 g/mol	211.25g/mol
Temperature (K)	200	200
Crystal system	orthorhombic	orthorhombic
Space group	Pca21	Pca21
a/Å	10.8946(4)	10.7087(5)
b/Å	13.0307(5)	12.0254(5)
c/Å	9.3686(3)	9.0344(4)
V/Å ³	1330.01(8)	1163.42(9)
Z	4	4
Density _{calc} /g/cm ³	1.195	1.206
Absorption coefficient (μ)/mm ⁻¹	0.074	0.076
F(000)	512	448
Crystal size/mm ³	0.06 x 0.25 x 0.51	0.18 x 0.29 x 0.50
Θ _{min} , Θ _{max} (°)	2.4, 28.3	3.4, 28.3
Dataset	-14:14, -17:17, -12:12	-14.14, -16.15, -11.12
Total uniq data, R(int)	18252,3320,0.027	36154, 2831, 0.018
R ₁ ^a (I > 2σ(I))	2918	2673
R, wR ₂ , S	0.0349, 0.0808, 1.04	0.0310, 0.0806, 1.03
Min and Max resd.dens.(e/ Å ⁻³)	-0.16,0.17	-0.19, 0.15

Table 2: Bond lengths and bond angles of the synthesized Schiff bases

PMP				TMP			
Bond lengths		Bond angles		Bond lengths		Bond angles	
O(1)-C(14)	1.350(2)	C(1)-N(1)-C(21)	118.58(15)	O(1)-(24)	1.3548(18)	C(2)-N(1)-(11)	116.20(12)
N(1)-C(1)	1.281(2)	C(14)-O(1)-(1A)	109.00	N(1)-C(2)	1.2740(18)	C(24)-O(1)-(1)	109.00
N(1)-C(21)	1.421(2)	N(1)-C(1)-C(11)	123.93(17)	N(1)-(11)	1.436(2)	N(1)-C(2)-(21)	125.01(13)
O(1)-H(1A)	0.8400	O(1)-C(14)-(15)	117.79(16)	O(1)-H(1)	0.8400	O(1)-C(24)-(23)	117.86(13)
C(1)-H(1A)	0.9500	C(11)-C(12)-(13)	121.25(16)	C(1)-(1A)	0.9800	C(11)-C(12)-13)	116.56(16)
C(25)-C(26)	1.384(3)	N(1)-C(1)-H(1)	118.00	C(25)-26)	1.381(2)	N(1)-C(2)-H(2)	117.00
C(24)-H(25)	1.391	C(12)-C(13)-(13)	120.00	C(26)-26)	0.9500	C(12)-C(13)-13)	119.00

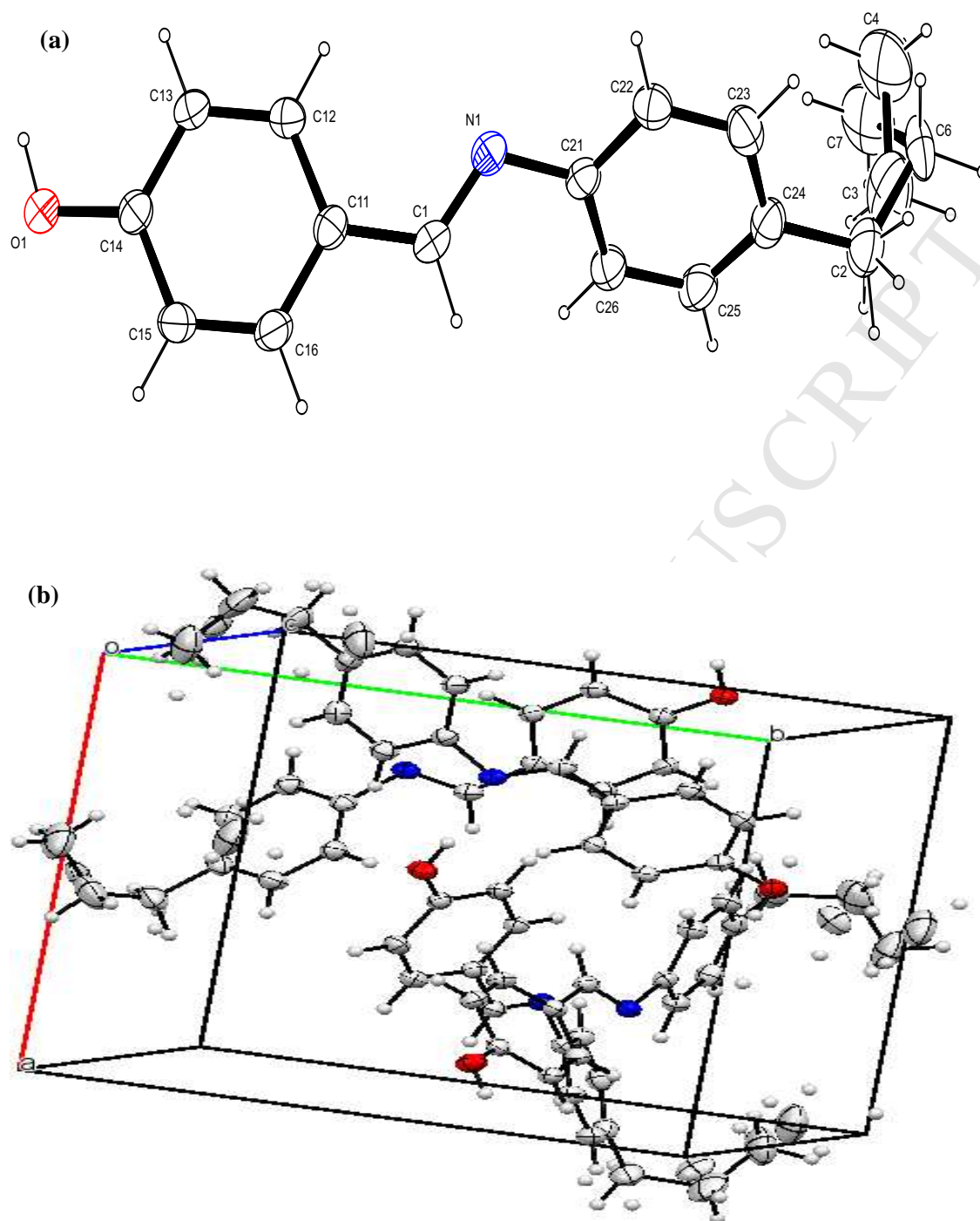


Figure 2: (a) Molecular structure of (E)-4-(((4-propylphenyl)imino)methyl)phenol with displacement ellipsoids drawn at 50% probability level, (b) Crystal packing drawn for the clearest view.

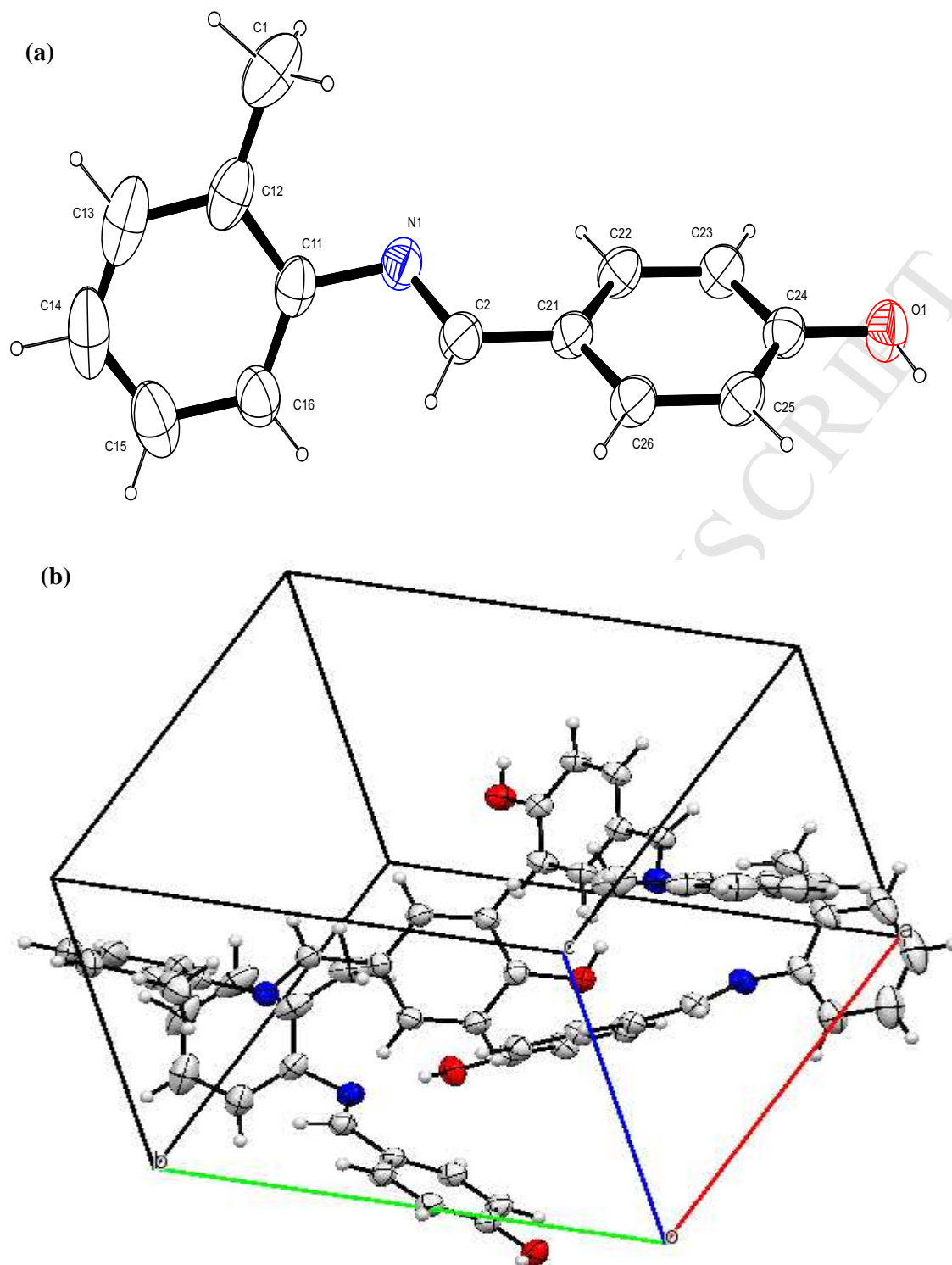


Figure 3: (a) The molecular structure of (E)-4-((2-tolylimino)methyl)phenol (TMP) with displacement ellipsoids drawn at 50% probability level, (b) Crystal packing drawn for the clearest view.

3.5 Electrochemistry of the studied compounds on mild steel

3.5.1 Potentiodynamic polarization studies

Polarization tests were conducted to probe the kinetics of the anodic and cathodic reactions [43]. Figure 4 presents the results of the effect of different concentrations of (PMP) and (TMP) on the cathodic and the anodic polarization curves of mild steel in 1 M HCl. The electrochemical data acquired from the polarization curves are presented in Table 3. Upon the addition of the Schiff bases, both the cathodic and anodic partial reactions were affected. Consequently, this caused a further reduction in the cathodic (β_c) and anodic current densities (β_a), and the resulting corrosion current density (i_{corr}). Therefore, the addition of PMP and TMP diminishes the anodic dissolution and also lessens the cathodic hydrogen evolution reaction [43]. As a result of recorded retardation of the cathodic and anodic current densities upon the addition of the compounds in the aggressive solution, they can be classified as a mixed-type inhibitor for the corrosion of MS in 1 M HCl [44, 45]. A close inspection of Figure 4 and E_{corr} values given in Table 3 reveals that the addition of the Schiff bases plays more active role on the cathodic arm of the Tafel plots in addition to the shifting of E_{corr} values towards more negative region, respectively. In addition, study conducted by Yadav *et al.* reported that the change in E_{corr} values above 85 mV suggests that a compound is an anodic or cathodic inhibitor [46]. In this present study, the highest displacement of E_{corr} was about 46.91 mV towards cathodic direction. These findings support the idea that the studied ligands function as a mixed-type inhibitor but with much more cathodic effect [44-47].

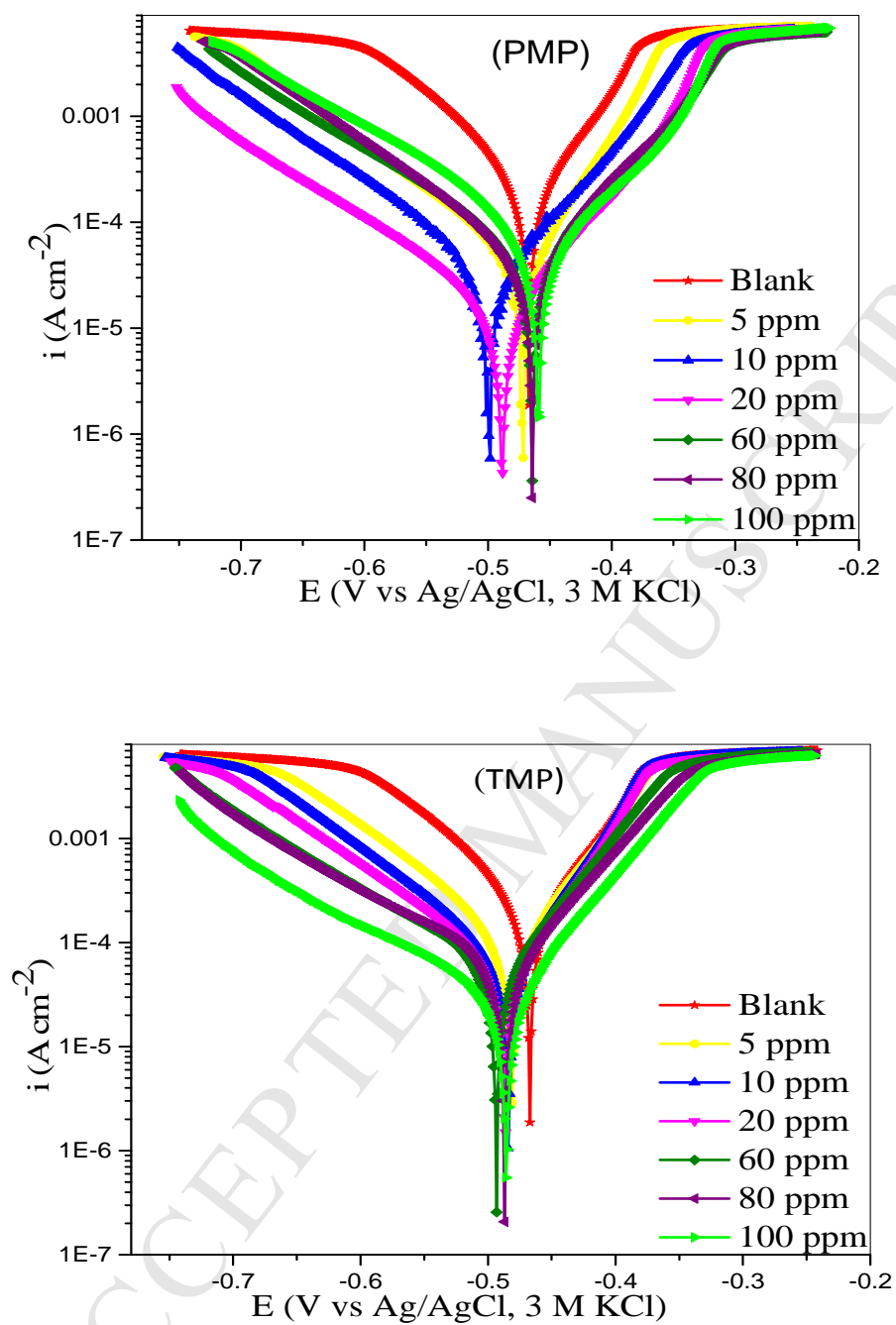


Figure 4: Polarization curves for mild steel in the absence (blank) and presence of different concentrations (in ppm) of PMP and TMP at 303 K.

Table 3: Tafel polarization parameters for MS in 1 M HCl solution in absence and at different concentration of the inhibitor ligands

Inhibitor	Conc (ppm)	β_a (mV/dec)	β_c (mV/dec)	$-E_{corr}$ (mV)	i_{corr} ($\mu\text{A cm}^{-2}$)	$\eta\%$
Blank	-	98.93	72.08	452.72	236.22	-
PMP	5	151.53	78.43	471.4	119.42	49
	10	84.33	123.62	499.63	39.24	83
	20	66.04	141.84	488.76	14.64	94
	60	48.43	62.99	464.33	14.62	94
	80	45.07	61.11	464.06	13.57	94
	100	38.86	54.82	459.34	8.74	96
TMP	5	127.72	80.90	481.76	164.74	30
	10	133.61	74.14	483.91	132.94	44
	20	54.44	122.1	486.59	54.53	77
	60	61.25	42.67	493.4	23.87	90
	80	58.98	31.88	486.98	20.22	91
	100	72.62	35.33	485.62	12.0	95

The inhibition efficiency ($\%IE_{PDP}$) presented in Table 3 was computed from the i_{corr} using the formula:

$$\%IE_{PDP} = 100 \left(1 - \frac{i_{corr}}{i_{corr}^0} \right) \quad (13)$$

Where i_{corr}^0 and i_{corr} are corrosion current densities in the absence and presence of inhibitors respectively.

Table 3 shows that as the inhibitor concentration increased, there was improved tendency of corrosion inhibition with corresponding decrease in corrosion current density. This trend can be attributed to the adsorption of inhibitor molecules on mild steel-acid interface which consequently shielded the metal surface from direct acid attack [46]. The lowest i_{corr} values which resulted to maximum inhibition efficiency obtained for PMP and TMP were 8.74 and 12.0 $\mu\text{A cm}^{-2}$ at 100 ppm inhibitor concentration, respectively.

3.5.2 Electrochemical impedance spectroscopy

Figure 5 shows typical Nyquist plots for mild steel (MS) in 1 M HCl in the absence and presence of different concentrations of PMP and TMP. All of the impedance spectra can be seen to display depressed semicircles with centres below the real axis. This characteristic unique property of Nyquist plot is caused by unavoidable roughness and inhomogeneity of metal electrodes that result during MS polishing [45, 48]. The inhibition efficiencies, $\%IE_{EIS}$, were calculated from Nyquist plots by the equation:

$$\%IE_{EIS} = 100 \left(\frac{R_{ct} - R_{ct}^0}{R_{ct}} \right) \quad (14)$$

where R_{ct} and R_{ct}^0 are the charge transfer resistance in the presence and absence of inhibitor respectively. Other derivable relevant impedance data are reported in Table 4. The impedance response of mild steel in 1 M HCl solution was greatly affected after the addition of all the ligands, and the impedance of the inhibited system improved significantly with increase in inhibitor concentration.

In addition, at 100 ppm concentration of ligands, larger diameter semicircles were significant compared to the other five lower concentrations of ligands (Fig. 5). In the presence of the Schiff base ligands, the entire Nyquist diagrams showed a diminished capacitive loop in the high frequency (HF) range and an inductive loop in the lower frequency (LF) range. The often observed HF capacitive loop has been ascribed to the charge transfer process and time constant of the electric double layer as well as the inhomogeneity of the surface which characterises numerous adsorption activities on metal [46]. Moreover, the LF inductive loop may be a result of the relaxation process obtained by adsorption of certain species, in this instance N and O on working electrode surface [49].

To ensure a proper interpretation of depressed semicircles with their foci below the real axis, a constant phase element (CPE) was introduced which is given by [46]:

$$Z_{CPE} = \left(\frac{1}{Y_0} \right) [(j\omega)^n]^{-1} \quad (15)$$

where, Y_0 is the CPE constant; ω is the angular frequency; j is the imaginary number and n is the phase shift (exponent). Figure 6 represents the equivalent circuit employed for the fitting of impedance spectra. Subsequently, the double layer capacitances, C_{dl} , for the circuit including a CPE were computed by using the following equation:

$$C_{dl} = (Y_0 R_{ct}^{1-n})^{1/n} \quad (16)$$

Other useful impedance parameters which includes R_s , R_{ct} , Y_0 , n and $\% \eta$ obtained from fitting the recorded EIS data using the equivalent circuit of Figure 6, are presented in Table 4. The data in Table 4 indicates that R_{ct} value improved significantly with the concentration of the Schiff bases. Consequently, the value of proportional factor Y_0 and C_{dl} obtained was decreased significantly upon the addition of inhibitor. However, no regular trend could be established across concentrations. Such anomaly may suggest that possible interaction of chemical species on MS surface cannot be ruled out, whereas the decrease in C_{dl} values connotes successful displacement of water molecules that have been found to have high dielectric constant [46]. The change in the values of R_{ct} and Y_0 can be related to the moderate displacement of water molecules by Schiff base molecules on the working electrode surface which eventually results to the reduction in the number of active sites exposed to corrosion [50]. The recorded increase in R_{ct} threshold values is usually ascribed to the formation of protective film on the metal/solution interface [43, 47]. The observed stability of n values within the range of 0.78-0.86 is an indication that the MS dissolution in the present report is hugely dependent on the charge transfer process [46]. In general, the results recorded for the inhibition efficiency of the two Schiff bases against MS corrosion in 1 M HCl using the EIS

technique are in tandem with those recorded using the PDP technique.

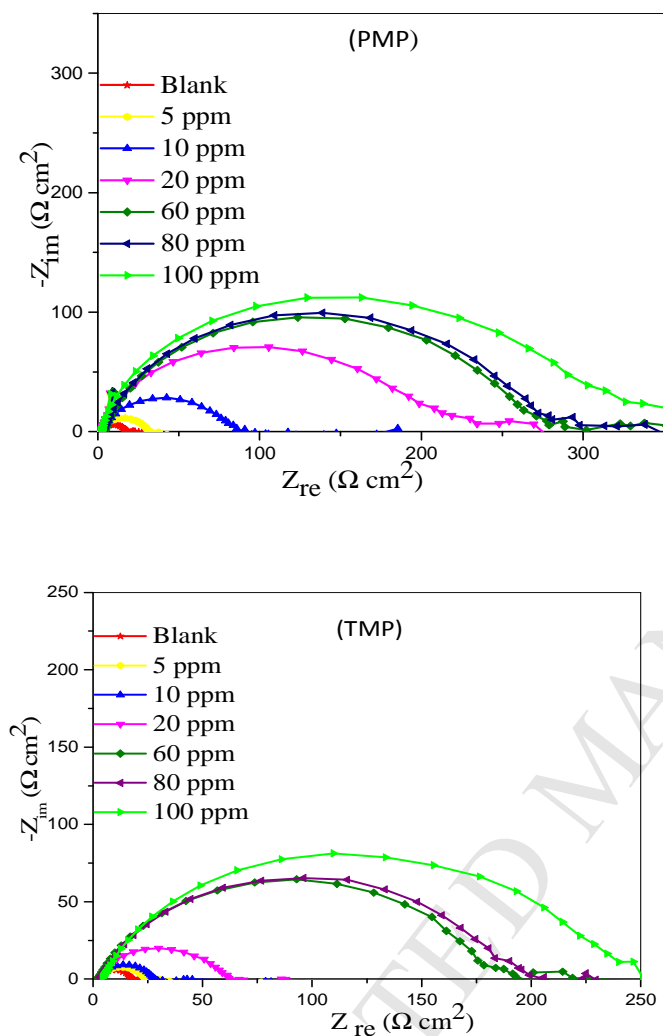


Figure 5: Nyquist plots for mild steel in the absence and presence of different concentrations of PMP and TMP at 303 K.

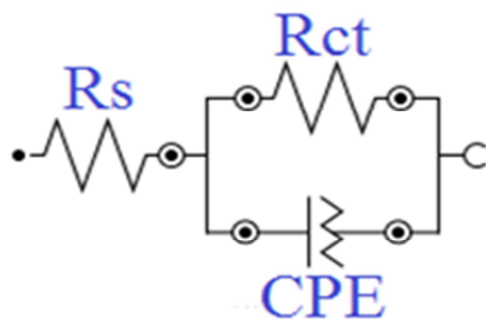


Figure 6: Equivalent circuit employed for the fitting of impedance spectra.

Table 4: Electrochemical impedance parameters obtained for MS in 1 M HCl in the absence and presence of different concentration of Schiff base ligands.

Inhibitor	Conc (ppm)	R_s ($\Omega \text{ cm}^{-2}$)	R_{ct} ($\Omega \text{ cm}^{-2}$)	Y_0 ($\mu\text{S s}^n \text{ cm}^{-2}$)	C_{dl} ($\mu\text{S s}^n \text{ cm}^{-2}$)	n	$\eta\%$
Blank	-	2.50	16.6	677	4000.8	0.84	-
PMP	5	2.02	32.9	457	2187.3	0.86	50
	10	3.35	92.8	241	2525.1	0.81	82
	20	2.11	236	169	1271.2	0.84	93
	60	4.13	291	116	981.6	0.83	94
	80	3.55	300	136	1196.4	0.83	94
	100	2.01	342	221	1375.8	0.86	95
TMP	5	3.59	22.9	496	3851.9	0.82	28
	10	2.88	28.7	483	3918.6	0.82	42
	20	3.38	67.6	371	2954.2	0.83	75
	60	2.50	199	175	2390.6	0.80	92
	80	3.35	211	143	2623.1	0.78	92
	100	4.22	267	129	2456.3	0.78	94

Figure 7 shows the Bode impedance modulus and phase angle plots for mild steel in 1 M HCl in the absence and presence of different concentration of the Schiff bases. The Bode plots depict a single peak as can be observed for phase angle against frequency. This observation entails that the dissolution of MS is determined by a single charge transfer process [51]. Furthermore, Daoud *et al.* alluded that this phenomenon is due to a single relaxation time constant [51]. At higher frequencies, it can be observed that the phase angle increased with resultant increase ascribed to the induction process involving the connecting cables [52]. In order to unravel the capacitive behaviour of the entire system under study, the relationship between $\log |Z|$ vs. $\log f$ at intermediate frequencies was explored, and presented in Table 5. It is obvious from the results presented in Figure 7 that at intermediate frequencies, there is a slight broadening of one time constant in the presence of inhibitor which could be due to the appearance of a surface film [46, 52]. Yadav *et al.* prescribed that an ideal capacitive behaviour would give a slope (S) of -1 and maximum phase angle (α) of -90 [46]. For the

present system at intermediate frequencies, the slope and maximum phase angle values in the range of -0.34 to -0.59; -52.17 to -69.30; and -0.49 to -0.62; -38.26 to -57.60 for PMP and TMP respectively were obtained. These deviations can be regarded as departure from the ideal capacitive behaviour at intermediate frequencies [46]. As a result of this, at increased concentrations, both PMP and TMP tend to attain steady state (of $-S$ and $-\alpha$) faster than in their absence. This behaviour reflects the catalytic activity of the two Schiff base ligands during the MS dissolution process [53].

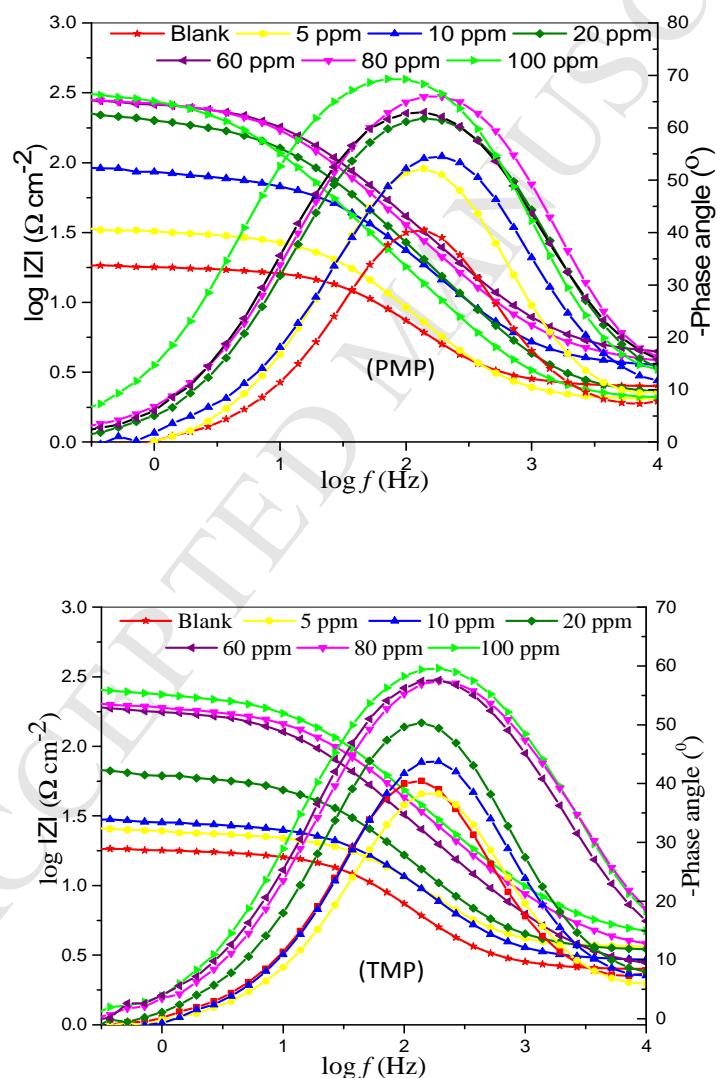


Figure 7: Bode impedance modulus and phase angle plots for mild steel in 1 M HCl in absence and presence of different concentration of PMP and TMP.

Table 5: The slopes of the Bode impedance magnitude plots at intermediate frequencies (S) and the maximum phase angles (α) for MS in 1 M HCl solution in the absence and presence of inhibitors.

Inhibitor	Concentration (ppm)	$-S$	$-\alpha$
Blank	-	0.30	40.47
	5	0.34	52.17
PMP	100	0.59	69.30
	5	0.49	38.26
TMP	100	0.62	57.60

3.6 Adsorption study

A good number of previous corrosion inhibition studies support the idea that metal samples in aqueous medium are usually covered with water dipoles adsorbed on the surface of the metal [44, 45, 54]. As a result, inhibitor molecules that eventually adsorb onto metal surface do so via a quasi-substitution mechanism. It is on this note that we subjected EIS data obtained in this research to two adsorption isotherms which includes Temkin (Fig. 8a) and Langmuir (Fig. 8b) models. Incidentally, the Langmuir isotherm produced the best fit from the experimental data. The Langmuir equation used in fitting the data is given by:

$$\frac{C_{inh}}{\theta} = \frac{1}{K_{ads}} + C_{inh} \quad (17)$$

where, θ is the degree of surface coverage; C_{inh} is the inhibitor concentration and K_{ads} is the equilibrium constant of the adsorption/desorption process. The choice of Langmuir over Temkin was based on the correlation coefficient (R^2) values closer to unity that were obtained for the Langmuir isotherm. In addition, an ideal Langmuir isotherm expects slope around unity [54], which is in line with values obtained in this study.

In order to attribute the adsorption process to either physisorption or chemisorption, the free energy of adsorption (ΔG_{ads}) was calculated for the Langmuir isotherm by making use of equation 18:

$$\Delta G_{ads} = -RT \ln(55.5 K_{ads}) \quad (18)$$

Where ΔG_{ads} is the standard free energy of adsorption; R is the gas constant and T is the absolute temperature. The value of 55.5 is the concentration of water in solution in molL^{-1} .

The values of K_{ads} and ΔG_{ads} are presented in Table 6. The obtained ΔG_{ads} values suggest that both PMP and TMP adsorb on mild steel surface in 1 M HCl via competitive physical and chemical adsorption mechanisms [45]. The negative sign mainly describes the spontaneity of the adsorption process [45, 54].

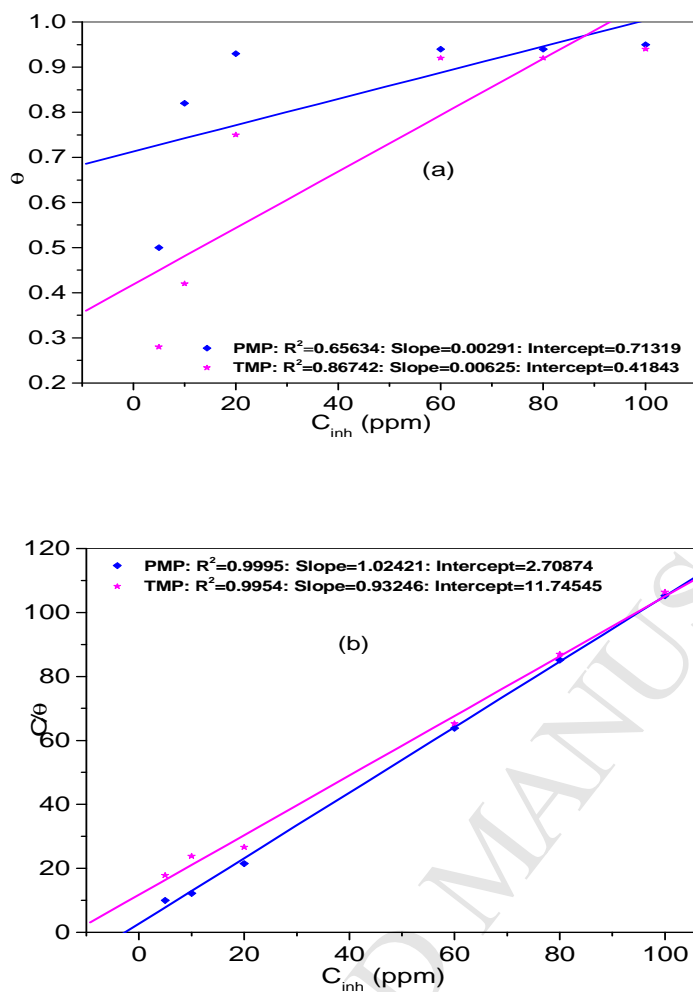


Figure 8: Representative adsorption isotherms for MS in 1 M HCl containing various concentrations of the studied Schiff base ligands: (a) Temkin and (b) Langmuir.

Table 6: Langmuir parameters representing the adsorption mechanism on mild steel surface obtained from EIS parameters at 303 K.

Inhibitor	$K_{ads} \times 10^3$	$-\Delta G^{\circ}_{ads}$ (kJ/mol)
PMP	88.340	38.81
TMP	17.987	34.80

3.7 Molecular interactions

The frontier molecular orbital and Fukui functions were used to explain the reactivity of the compounds and their various interactions with the surface of the metal. The optimized structures, highest occupied molecular orbital (HOMO), lowest unoccupied molecular orbital (LUMO) and the Fukui indices of the Schiff base molecules are presented in Figure 9. Other quantum chemical parameters as shown in Table 7 were basically calculated from the E_{HOMO} and E_{LUMO} . The activity of the molecules is determined by the E_{HOMO} and E_{LUMO} . The higher value of E_{HOMO} shows its readiness to donate electrons and form coordinate covalent bonds with the empty d-orbitals of the metal atoms thereby enhancing the corrosion inhibition effect. From the studied molecules, PMP has higher E_{HOMO} and reasonably low E_{LUMO} values that afford it the ability to donate and accept electrons under favourable conditions than TMP.

The energy gap ΔE is smaller in PMP compared to TMP signifying that it is unstable, more polarised, of higher reactivity and can easily be adsorbed on the metal surface than TMP [46]. The values of the dipole moment are supposed to support the other parameters in the sense that molecules with higher dipoles reflect stronger dipole-dipole interactions with metal surfaces. In other words, PMP should have a higher dipole moment than TMP, however, there are some reports which show that experimental inhibition efficiencies sometimes do not conform to the values of the dipole moments [55-58]. From the Figure 9, there is better electron distribution in TMP compared to PMP which attest to the value of the dipole moment that measures the polarity of the molecules. The propyl and methyl groups attached to the para and ortho positions of the backbone molecule respectively have played a significant role in affecting the surface layer of the molecules. Our result in this research therefore shows that decrease in dipole moment increases the inhibition efficiency which is adequately supported by the experimental results. Furthermore, other quantum chemical

parameters such as chemical potential, global softness, nucleophilicity index and the number of electrons transferred during the adsorption shows higher values for PMP than TMP, thereby confirming the enhanced electron releasing ability of the compound [44, 46, 55].

Apart from the high protective performance offered by the synthesized Schiff base inhibitors which is attributed to the effect of the phenyl and azomethine group ($-\text{C}=\text{N}-$) in their moiety; contributing inhibition efficiency could equally be evident from electron-donating groups attached to the molecules due to their ability to furnish the π -system with more electrons [59, 60]. PMP and TMP have nearly the same size and similar active centres, but PMP exhibits higher inhibition efficiency than TMP due to a higher delocalized electrons emanating from the propyl attachment than from the methyl.

The local reactivity of the molecules was probed by exploring their Fukui function as a measurement of the chemical reactivity; a means to ascertain the reactive regions, that is, the electrophilic behaviour of the molecule. We observe that the f^- function corresponds to a certain extent with the HOMO-LUMO locations, indicating the site that is most susceptible to electrophilic attacks are the π electron centres delocalized over the entire aromatic rings in both molecules [47]. In addition, the propyl attachment in PMP is also favourable.

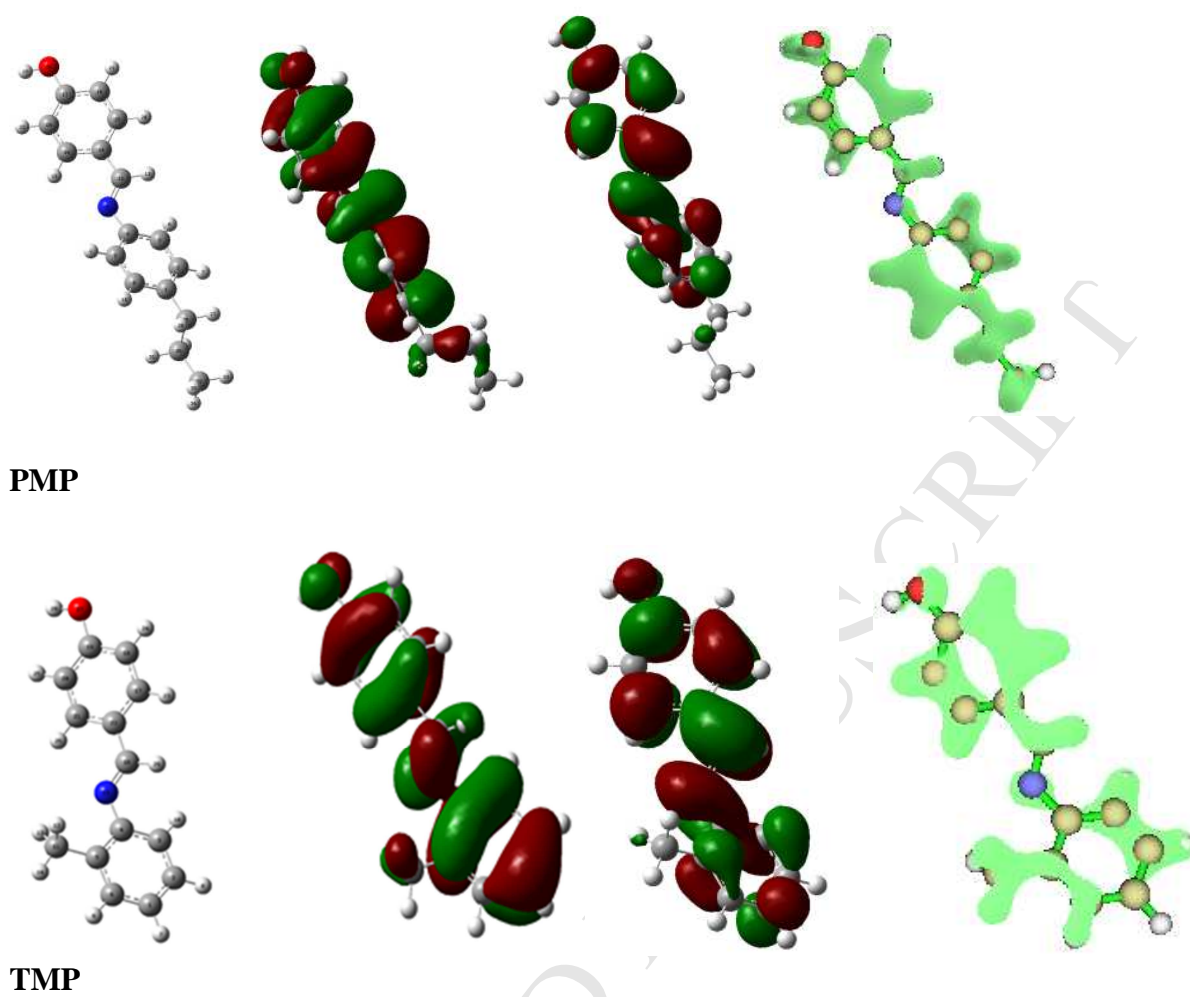


Figure 9: Optimized structures, HOMO, LUMO and Fukui (f^-) indices for the studied compounds

Table 7: Quantum chemical parameters for the synthesized Schiff base compounds.

compound	(Z)-4-(((4-propylphenyl)imino)methyl)phenol	(E)-4-((o-tolylimino)methyl)phenol
Dipole moment(debye)	0.7172	1.5561
E_{HOMO} (eV)	-5.8357	-5.9130
E_{LUMO} (eV)	-1.6944	-1.7189
ΔE (eV)	4.1413	4.1941
Ionization potential(lp)	5.8357	5.9130
Electron affinity (Ea)	1.6944	1.7189
Chemical potential(μ)	-3.7651	-3.8159
Absolute hardness(χ)	2.0706	2.0970
Global softness(σ)	0.4829	0.4768
Nucleophilicity index(N)	0.2921	0.2880
Fraction of electron transferred (ΔN)	0.7811	0.7591

Conclusion

Schiff base compounds are environmentally benign ligands and have been synthesized in this report. The spectroscopic analysis of the compounds revealed the characteristic imine functional groups, and the mass spectra confirmed the molecular masses of the compounds as 240 g/mol (PMP) and 212 g/mol (TMP). The structural analysis revealed intermolecular O1—H1A...N1i (i: -x,1-y,1/2+z) interaction of length 1.88 Å for PMP and intermolecular O1—H1...N1i (i: 1/2+x,1-y,z) interaction of length 1.92 Å which links adjacent molecules and can be described with a C11(8) graph-set descriptor on the unary level. Both compounds crystallized as orthorhombic, and TMP showed a disordered propyl group over two positions in 0.79:0.21 ratios. The C=N bond lengths are 1.281 Å and 1.274 Å for PMP and TMP

respectively. The corrosion inhibition efficacies of the synthesized compounds were investigated; and from Potentiodynamic polarization, electrochemical impedance spectroscopy, adsorption isotherms and quantum chemical calculations, the following conclusions were made:

1. At higher concentration of the ligands (100 ppm), Nyquist plots with larger diameter semicircles than the other five lower concentrations of the compounds were obtained. This showed increased inhibition and the percentages obtained for the two compounds were approximately the same. The results of potentiodynamic polarization and electrochemical impedance were in tandem with each other.
2. The obtained ΔG_{ads} values suggest that both PMP and TMP adsorbed on mild steel surface in 1 M HCl via competitive physical and chemical adsorption mechanisms with favourable compliance to Langmuir model.
3. The quantum chemical parameters and Fukui indices revealed that PMP and TMP have nearly the same size and similar active centers but PMP exhibits a little higher inhibition efficiency than TMP due to a higher delocalized electrons emanating from the propyl attachment than from the methyl. The Fukui isosurface diagrams showed the delocalisation of π -electron system over the aromatic rings.

With the results obtained from this research, the properties of the compounds are now known and their behaviour as corrosion inhibitors could be assessed with similar compounds in order to step up the search for more efficient green corrosion inhibitors.

References

1. H. Iranmanesh, M. Behzad, G. Bruno, H. A. Rudbari, H. Nazari, A. Mohammadi, O. Taheri, *Inorg. Chim. Acta* 395 (2013) 88.
2. G. Yadav and J. V. Mani, *Int. J. Sci. Res.* 4(2015)127.
3. G. Vanangamudi, S. P. Sakthinathan, R. Suresh, V. Mala, K. Sathiyamoorthi, D. Kamalakkannan, K. Ranganathan, S. J. Joseph, G. Thirunarayanan, *Int.J.Sci.Res. know.* 1 (2013) 483.
4. H. J. Yang, W. H. Sun, Z. L. Li and M.A. Zhi, *Chin. Chem. Letts.*, 13 (2002)6.
5. A. C. Tella, U. B. Eke, S. O. Owalude, J. Saudi Chem. Soc. (2013) <http://dx.doi.org/10.1016/j.jscs.2012.12.013>.
6. N.D. Chaudhary, *Bibechana* 9 (2013) 80.
7. K. K. Upadhyay, A. Kumar, S. Upadhyay and P. C. Mishra *J. Mol. Struct.* 873 (2008) 16.
8. P.G. Baraldi, M.G. Pavani, M. Nunez, P. Brigidi, B. Vitali, R. Gambari, R. Romagnoli, *J. Med. Chem.* 10 (2002) 456.
9. M.M Kandeel, S.M. Ali, E.K.A. Abed El Ali, M.A. Abdelgawad, P.F. Lamie, *J. Chem. Pharm. Res.* 4 (2012) 4106.
10. R.V. Antre, A. Cendilkumar, D. Goli, G.S. Andhale and R.J. Oswal, *Saudi Pharm. J.* 19 (2011) 243.
11. S.M. Sondhi, M. Johar, S. Rajvanshi, S.G. Dastidar, R. Shukla, R. Raghbir, J.W. Lown, *Aust. J. Chem.* 54 (2001) 74.
12. M.N. Nasr, M.M. Gineinah, *Arch. Pharm. Res.* 335 (2002) 289.
13. M.S. Chowdhury, M.M. Matin, M.N. Anwar, *Chittagong Univ. Stud. Part II Sci.*, 21 (1997) 83.
14. K.S. Parikh and S.P. Vyas, *Int. J. Pharm. Sci. Res.* 3(2012) 3427.

15. N.P. Singh, A.N. Srivastava, *Asian J. Chem.* 25 (2013) 537.
16. M.M. Kandeel, S.M. Ali, E.K.A. Abed El Ali, M.A. Abdelgawad, P.F. Lamie, *Org. Chem. Indian J.* 9 (2013) 91.
17. D. M. Boghaei, E. Askarizadeh, A. Bezaatpour, *Spectrochim. Acta*, 69 A (2008) 628.
18. Y. Prashanthi, K. Kiranmai, N. J. Subhashini, P. Shivaraj, *Spectrochim. Acta* 70 A (2008) 35.
19. K. Tanaka, R. Shimoura, M. R. Cairra, *Tetrahedron Lett.* 51 (2010) 452.
20. G. Pistolis, D. Gegiou, E. Hadjoudis, *J. Photochem. Photobiol.* 93A (1996) 184.
21. J. H. Jia, X. M. Tao, Y. J. Li and W. J. Sheng, *Chem. Phys. Lett.* 514 (2011) 118.
22. A. M. A. Ibrahim, *Thermo-chim. Acta* 197 (1992) 217.
23. S. Kumar, D. N. Dhar, P. N. Saxena, *J. Sci. Ind. Res.* 68 (2009) 187.
24. M. A. Ashraf, K. Mahmood, A. Wajid, *IPCBEE*, 10 (2011) 7.
25. K.C. Emregül, E. Düzgün, O. Atakol, *Corr. Sci.* 48 (2006) 3260.
26. V. Krishnakumar, N. Prabavathi, S. Muthunatesan, *Spectrochim. Acta* 69A (2008) 533.
27. M. Karabacak, D. Karagoz, M. Kurt, *J. Mol. Struct.* 892 (2008) 31.
28. T. Rajamani, S. Muthu, M. Karabacak, *Spectrochim. Acta* 108A (2013) 196.
29. M. Karabacak, M. Kurt, A. Atac, *J. Phys. Org. Chem.* 22 (2009) 330.
30. N. K. Gupta, M. A. Quraishi, C. Verma, A. K. Mukherjee, *RSC Adv.* 6 (2016) 102087.
31. APEX2, SADABS and SAINT, Bruker AXS Inc., Madison, Wisconsin, USA, 2010.
32. G. M. Sheldrick. A short history of SHELX. *Acta Cryst.* 64A (2008) 122.
33. C. B. Hübschle, G. M. Sheldrick and B. Dittrich. ShelXle: a Qt graphical user interface for SHELXL. *J. Appl. Cryst.*, 44 (2011) 1284.
34. M.J. Frisch, G.W. Trucks, H.B. Schlegel, G.E. Scuseria, M.A. Robb, J.R. Cheeseman, J.A. Montgomery, T. Vreven, K.N. Kudin, J.C. Burant, J.M. Millam, S.S. Iyengar, J.

- Tomasi, V. Barone, B. Mennucci, M. Cossi, G. Scalmani, N. Rega, G.A. Petersson, H. Nakatsuji, M. Hada, M. Ehara, K. Toyota, R. Fukuda, J. Hasegawa, M. Ishida, T. Nakajima, Y. Honda, O. Kitao, H. Nakai, M. Klene, X. Li, J.E. Knox, H.P. Hratchian, J.B. Cross, V. Bakken, C. Adamo, J. Jaramillo, R. Gomperts, R.E. Stratmann, O. Yazyev, A.J. Austin, R. Cammi, C. Pomelli, J.W. Ochterski, P.Y. Ayala, K. Morokuma, G.A. Voth, P. Salvador, J.J. Dannenberg, V.G. Zakrzewski, S. Dapprich, A.D. Daniels, M.C. Strain, O. Farkas, D.K. Malick, A.D. Rabuck, K. Raghavachari, J.B. Foresman, J.V. Ortiz, Q. Cui, A.G. Baboul, S. Clifford, J. Cioslowski, B.B. Stefanov, G. Liu, A. Liashenko, P. Piskorz, I. Komaromi, R.L. Martin, D.J. Fox, T. Keith, M.A. Al-Laham, C.Y. Peng, A. Nanayakkara, M. Challacombe, P.M.W. Gill, B. Johnson, W. Chen, M.W. Wong, C. Gonzalez, J.A. Pople, Gaussian 03W, Revision E. 01, Wallingford, CT, Gaussian Inc (2004)
35. S. Martinez, *Mater. Chem. Phys.* 77 (2003) 102.
36. T. Koopmans, *Über die Zuordnung von Wellenfunktionen und Eigenwerten zu den Einzelnen Elektronen Eines Atoms*, *Physical* (1934) 113.
37. D.P. Singh, V. Grover, K. Kumar, K. Jain, *J. Serb. Chem. Soc.* 76 (2011) 393.
38. R. M. Issa, A. M. Khedr, H. Rizk, *J. Chin. Chem. Soc.* 55 (2008) 884.
39. W. Kemp, *Organic spectroscopy*, Macmillian press London (1991) 71.
40. J. Bernstein, R. E. Davis, L. Shimoni, N.L. Chang, *Angew. Chem. Int. Ed. Engl.* 34 (1995) 1573.
41. M. C. Etter, J. C. MacDonald, J. Bernstein, *Acta Crystallogr.* 46B (1990) 262.
42. A. Soltani, F. Ghari, A. D. Khalaji, E. T. Lemeski, K. Fejfarova, M. Dusek, M. Shikhi, *Spectrochim. Acta* 139A (2015) 278.
43. H. H. Hassan, E. Abdelghani, M. A. Amin, *Electrochim. Acta* 52 (2007) 6366.
44. N.O. Eddy, H. Momoh-Yahaya, E. E. Oguzie, *J. Adv. Res.* 6 (2015) 217.

45. H.U. Nwankwo, C.N. Ateba, L.O. Olasunkanmi, A.S. Adekunle, D.A. Isabirye, D.C. Onwudiwe, E.E. Ebenso, *Mater.* 9 (2016) 19.
46. D. K. Yadav, M.A. Quraishi, B. Maiti, *Corros. Sci.* 55 (2012) 266.
47. J. Saranya, P. Sounthari, K. Parameswari, S. Chitra, *Measurement*, 77 (2016) 186.
48. A.K. Satapathy, G. Gunasekaran, S.C. Sahoo, K. Amit, P.V. Rodrigues, *Corros. Sci.* 51 (2009) 2856.
49. I. Ahamad, R. Prasad, M.A. Quraishi, *Corros. Sci.* 52 (2010) 942.
50. F. Bentiss, M. Lebrini, M. Lagrenee, M. Traisnel, A. Elfarouk, H. Vezin, *Electrochim. Acta* 52 (2007) 6872.
51. D. Daoud, T. Douadi, S. Issaadi, S. Chafaa, *Corros. Sci.* 79 (2014) 58.
52. L. O. Olasunkanmi, M. M. Kabanda, E. E. Ebenso, *Physica E*, 76 (2016) 126.
53. H. H. Hassan, *Electrochim. Acta* 53 (2007) 1730.
54. A. Ostovari, S.M. Hoseinie, M. Peikari, S.R. Shadizadeh, S.J. Hashemi, *Corros. Sci.* 51 (2009) 1949.
55. L.C. Murulana, A.K. Singh, S.K. Shukla, M.M. Kabanda, E.E. Ebenso, *Ind. Eng. Chem. Res.* 51 (2012) 13299.
56. G. Gece, *Corros. Sci.* 50 (2008) 2992.
57. A. Rochdi, O. Kassou, N. Dkhireche, R. Touir, M. El Bakri, M. EbnTouhami, M. Sfaira, B. Mernari and B. Hammouti, *Corros. Sci.* 80 (2014) 452.
58. S. Kumar, H. Vashisht, L. O. Olasunkanmi, I. Bahadur, H. Verma, G. Singh, I. B. Obot, E. E. Ebenso, *Sci. Reports* 6 (2016) 18.
59. A. I. Adawy, M. A. Abbas, K. Zakaria, *Res. Chem. Intermed.* 42 (2016) 3411
60. M. Yadav, D. Behera, S. Kumar, P. Yadav, *Chem. Eng. Comm.* 202 (2015) 315.

Highlights

- (E)-4-(((4-propylphenyl)imino)methyl)phenol and (E)-4-((2-tolylimino)methyl)phenol were synthesized
- The crystal structures of the two synthesized Schiff bases were reported
- The experimental and theoretical data were correlated using DFT calculations
- The corrosion inhibition behaviour of the two Schiff bases were studied